# Cyber Prostheses: How to Turn Medical Implants into Wireless Data Generators for Healthcare 4.0

**C. Occhiuzzi, *Member, IEEE*, F. Lestini, A. Mostaccio, F. Naccarata, F.M.C. Nanni, and G. Marrocco, *Senior Member, IEEE*,**

*Pervasive Electromagnetics Lab, DICII-University of Roma "Tor Vergata", Via del Politecnico 1 00133 Roma, www.pervasive.ing.uniroma2.it, cecilia.occhiuzzi@uniroma2.it*

Manuscript received …..; revised ……. . First published ……..Current version published …... This research was partially sponsored by …….

**Abstract:** The evolution of prosthetics has been significantly shaped by advancements in biomedical engineering and state-of-the-art technologies. A notable breakthrough in this domain is the emergence of wireless implantable devices, representing a transformative shift in implant design and functionality. These prostheses aim to restore lost functionalities and seamlessly integrate with the human body, offering therapeutic and diagnostic capabilities when equipped with embedded sensors. However, wireless prostheses require *through-the-body* communication links with external readers, achieved through minimal structural alterations to preserve core functionalities and without batteries and complex electronics for biocompatibility and miniaturization. Such challenges can be addressed through two approaches: utilizing the prosthesis structure as a radiating element according to the paradigm of structural antennas and employing passive, battery-less communication platforms operating in backscattering. The feasibility of these approaches, focusing on the UHF band (860-960 MHz), is here demonstrated through theoretical formalization, case studies, and in-vitro measurements, with insights into materials and manufacturing processes provided.

**Index Terms:** Implanted antenna, RFID, wireless prostheses.

## 1. Introduction

Human prosthetics have undergone remarkable transformations over the years, driven by advancements in biomedical engineering and cutting-edge electronic technologies. Wireless implantable prostheses, in particular, represent a paradigm shift in artificial implants design [1]. These devices restore lost functionalities and integrate seamlessly with the human body, offering therapeutic and diagnostic capabilities when embedded with sensors [2]. These sensors monitor parameters such as temperature, pressure, strain, pH levels, and specific biomarkers, providing comprehensive insights into patient and implant conditions [3], [4]. The real-time data generated enhances diagnostic accuracy and enables timely intervention and personalized treatment, even in the event of implant failure [5].

For effective data collection, a through-the-body wireless communication link is essential to collect energy and exchange data. This requires the implanted prosthesis to host an integrated antenna and necessary electronics. Recent examples include a conformal patch antenna in a hip implant for self-monitoring at 2.4 GHz [6], an active wireless system at 400 MHz in a femoral prosthesis [7], and a fully bioresorbable wireless nerve stimulator [8].

Maintaining the core functionalities of the prosthesis while adding new features is crucial. This necessitates minimal mechanical alterations to avoid comprehensive requalification. Antenna design, therefore, requires unconventional strategies tailored to the implant's topology, material, and site of operation. The big challenge is to avoid the use of battery to improve the device safety and reliability, mitigating concerns related to battery longevity [9], upkeep, and potential intra-body hazards [10].

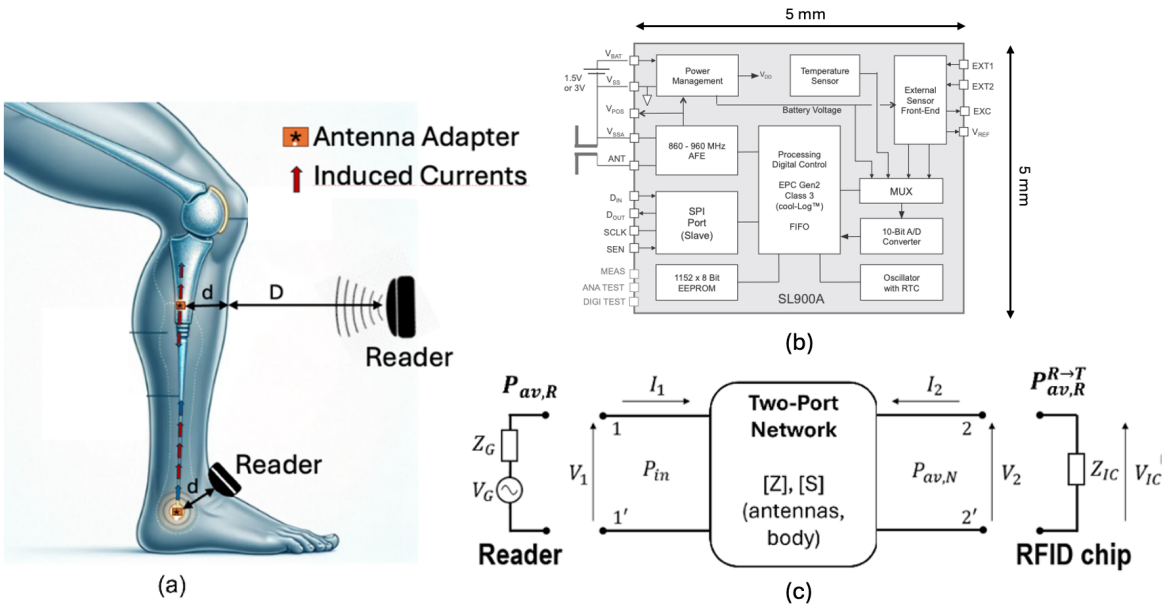


*Figure 1 a) Scheme of the RFID-based through-the-body communication link, b) Basic block diagram of an RFID sensing IC (adapted from AMS_SL900A Datasheet) and b) through-the-body communication link equivalent electrical representation.*

Two complementary strategies address these constraints. The first involves exploiting the prosthesis structure itself as a radiating element, borrowing methodologies from avionic and naval systems [11]. In this sense, the prosthesis acts as an antenna, intercepting electromagnetic fields from an external receiver and transferring power to the core electronics for sensing purposes (see Fig 1 a). The second strategy establishes through-the-body communication links based on passive and battery-less platforms, such as Radio Frequency Identification (RFID) [12]. RFID technology uses a backscattering-based communication protocol between an external reader and an Integrated Circuit (IC) within the prosthesis [13]. Modern ICs also integrate digital sensors and analog/digital ports for external devices [14], enabling the monitoring of temperature [15], humidity [16], strain [17], and biochemical analysis of the surrounding environment [18], [19]. RFID technology hence plays a pivotal role in the development of zero-power sensorized prostheses by eliminating the need for onboard batteries and minimizing the complexity of required electronics. Since all essential components for monitoring and communication are integrated within the IC (see Fig 1 b), the objective of achieving low-impact and low-complexity architectures can be reasonably achieved.

This paper is a tutorial on designing integrated telemetry systems for smart passive implants. It provides theoretical formalization and performance parameters for evaluating the communication link (Section II), classification of prostheses from an electromagnetic perspective, and guiding strategies for adding radiation features. Attention is primarily given to impedance matching between the medical device and integrated electronics, that is crucial for effective communication. Indeed, radiation gain is influenced by the prosthesis layout, available space, and the environment surrounding the implant, i.e., the lossy human body. The study explicitly refers to RFID passive communication platforms operating in the UHF (860-960 MHz) band. Compared to other link options (HF 13.56 MHz [20], MedRadio 403 MHz, ISM microwave 2.45 GHz [21]), this frequency band can simultaneously enable reasonable penetration depth, antenna miniaturization, and battery-less data exchange. The methodologies for turning conventional implants into Cyber-prostheses are described through realistic case studies, numerical analysis, and early in-vitro measurements, (Sections III-IV). Finally, insights into materials and manufacturing processes complete the analysis (Section V).

## 2. Rationale of the Cyber Implants

We will hereafter denote "cyber prosthesis" as an advanced medical implant designed to both restore

impaired bodily functions and wirelessly monitor physiological parameters, thereby providing real-time information about the implant's status and the patient's health. These capabilities are achieved through subtle modifications of the layout, materials, and components, integrating electronic and communication elements into the implant. Specifically, the metallic and dielectric portions of the prostheses are transformed into radiating and supportive elements to accommodate necessary sensors and the RFID integrated circuit (IC). The IC oversees sensing activity and data transmission without needing a local power supply, harvesting and backscattering power from the field provided by the external reader (Fig. 1a). To minimize structural modifications, the IC is integrated into the implant through an adapter coupled to the radiating element, ensuring impedance matching between the IC and the object. The *antennification* of prostheses involves selecting the most suitable portion of the layout to host either the adapter or the entire radiating element. In both cases, one or more ICs can be included for multi-sensing or distributed measurement.

Depending on their shape, materials, and size, various antenna-equivalent configurations can be identified for prostheses, as summarized in Table I and illustrated in Fig. 2. Metallic prostheses can be categorized as either volumetric or linear. Volumetric metal implants, such as joint prostheses, typically have bulky geometries well-suited to act as ground planes and cavities for the antenna's adapter. In these instances, the adapter can be connected to the implant via notches or slots carved into less mechanically stressed areas. The extent of these modifications is determined through a mechanical/electromagnetic co-design using multiphysics simulations.
Conversely, linear metal implants like nails, stents, or bone plates can support longitudinal current patterns like wire antennas, such as loops and dipoles. The adapter can be placed either at the center or extremities of the prosthesis, creating balanced or unbalanced antennas, respectively. The adapter can be accommodated within fastening holes, secured at the interface for modular implants, or simply coupled to the implant without disrupting its integrity. In these cases, the assembly can utilize the existing biocompatible coating of the medical device or incorporate a specialized coating for the antennification of the implant.

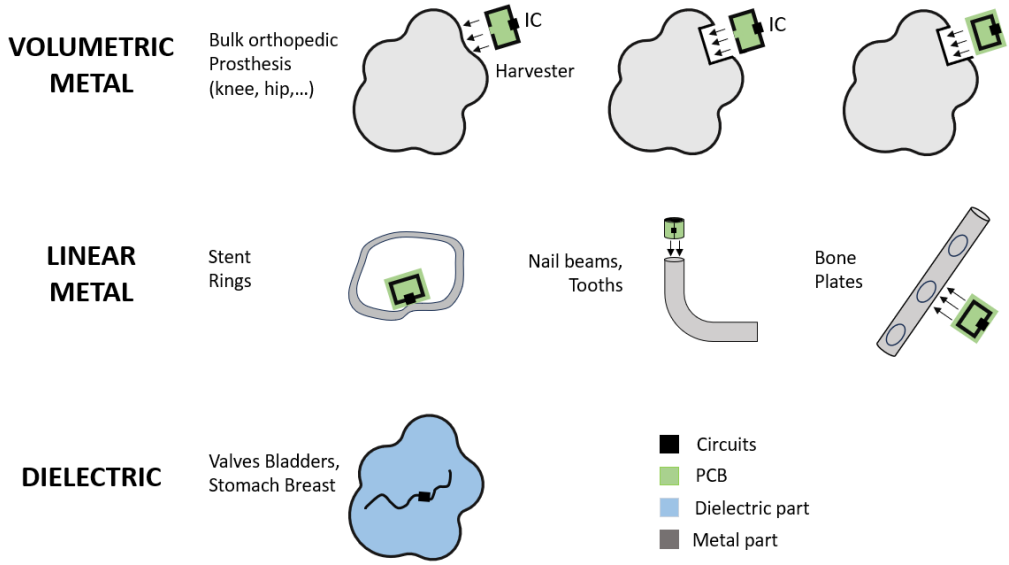


*Figure 2 Schematic representation of the different* antennification *strategies depending on the nature of the implant (metallic/dielectric, linear/bulk) and the layout of the adapter (loop/T/Gamma-match, end-cap, notch).*

Finally, polymeric or ceramic implants, or their sections, can accommodate electronics and conductive materials, serving as substrates for external radiating elements.

The adapter can be shaped in various forms, such as Loop-match [22], T-match [15], Gamma-match [23], End-cap [24], and Notch [25], [26]. These exciters, besides incorporating the RFID IC, may also integrate discrete tuning elements to address impedance matching requirements. This is especially crucial when human variability significantly affects communication features [27].

In the following sections, the classification in Tab.1 is adopted to describe the different Cyber-prostheses realizations.

*Table 1 Classification of the implants from an antenna perspective*

| Type of protheses | Example | | Antenna equivalent |
|---|---|---|---|
| *Volumetric Metal* | Hip/knee prostheses, Plate | 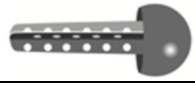 | Dipole, loop, cavity-backed antenna, |
| *Linear Metal* | Nail, Valves, Stent, dental implant |  | |
| *Dielectric* | Abdominal graft, metal-free valve | 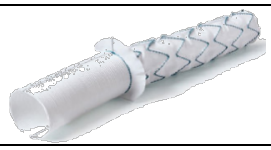 | Substrate hosting wire antennas |

### 2.1. Communication link

Due to the small distance (*d+D)* between the implant and the external reader (Fig.1 a) and to the effects of the human body, a typical through-the-body communication link can be described through a mid-field interaction and properly modeled [28] by a two-ports network (Fig.1 c). Here $Z_{ii}$ and $Z_{ij}$ are the self and mutual impedances of the communication elements, namely the implanted antenna (Port 2) and the external reader (Port 1). $Z_G$ and $Z_{chip}$ are the impedance of the generator connected to the reader antenna and the IC impedance, respectively.

Considering the backscattering-based UHF RFID protocol, the two-way, forward and backward, backscattering link [29] can be parameterized through the Transducer Power Gain $G_T$ and Round-Trip Power Gain $G_{RT}$. A reliable communication link can be established if the power emitted by the reader ($P_{av,R}$) simultaneously *i)* activates the implanted transponder, *ii)* generates a backscattered signal strong enough to be detected by the reader's receiver, and *iii)* complies with SAR (Specific Absorption Rate) limits inside the body. For the current power sensitivities of state-of-the-art ICs ($p_C$) and receivers ($p_R$), the through-the-body communication link is established if the power $P_{av,R}^{R\to T}$ delivered by the reader to the transponder's chip exceeds the chip sensitivity $p_C$. The lowest available power threshold $P_{av,R}^{min}$ at the reader to activate the transponder is (parameters expressed in dB):

$$P_{av,R}^{min} > P_{av,R}^{R\to T}\big|_{dB} = p_C - G_T \tag{1}$$

with

$$G_T = \frac{P_{R\to T}}{P_{av,R}} = \frac{4R_{chip}R_G|Z_{21}|^2}{|(Z_{11}+Z_G)(Z_{22}+Z_{chip})-Z_{12}Z_{21}|^2} \tag{2}$$

By denoting with $P_{av,R}^{max}$ the maximum available power of the generator (typically 1 W [30]), the following constrained power margin *M* of the link is introduced:

$$M(p_C, G_R) = min\{P_{av,R}^{max}, P_{av,R}^{SAR}\} - P_{av,R}^{min} - P_0 \tag{3}$$

with $P_{av,R}^{SAR}$ the maximum available power from the reader so that the corresponding SAR in the body is compliant with the regulation [31], and $P_0$ a safe value to account for non-fully controllable parameters of the system. Therefore, communication can be established and reliable for a specific implanted transponder if M >0. It is worth noticing that being the communication link extremely weak, RFID ICs operate close to the threshold level. Consequently, non-linearities in the IC's operation, such as input impedance variability [32], [33], have minimal impact on the link and were hereafter omitted for simplicity. Moreover, modern ICs include some self-indicators, such as the on-chip power [33] to

ensure that sensing data remains accurate. This indicator can be hence used to dynamically adjust the power feeding the reader so that the non-linear regime can be avoided.
In case the distance between the implanted device and the external reader antenna is such to reach the far-field condition (i.e. namely the reader is placed outside the body at a distance $D > \sim\lambda/2$, with $\lambda$ the wavelength) the Transducer Power Gain $G_T$ can be expressed through the Friis formula [34] and the Realized Gain $G_\tau$ of the cyber-prosthesis, i.e. the gain of the implanted antenna scaled by the mismatch with the IC impedance, can be defined:

$$G_\tau = \frac{G_T}{\chi}\left(\frac{4\pi(d+D)}{\lambda}\right)^2 \tag{4}$$

with $\chi$ polarization loss factor between reader and prosthesis antennas.
For instance, with $p_C$ =-15dBm and $P_{av,R}^{max}$ =30dBm, the resulting values of *M* for different IC locations typically range between 2 and 6 dB [29]. Implants placed up to 7-10 cm inside the body can be easily reached [22], even for extremely miniaturized configurations implanted in high lossy medium like human blood. For more superficial implants, instead, the reader antenna can be even placed far from the body, up to 40 cm away, allowing remote monitoring of multiple subjects in domestic environments [29]. In these cases, typical values of the realized gain ranges between -35dB and -25dB [35].

Depending on the through-the-body link configuration (mid field or far field) the performance parameters $\{P_{av,R}^{min}, d, D, G_T, M \text{ and } G_\tau\}$ can be used to evaluate the communication capabilities of the cyber-protheses. Five of these parameters $\{P_{av,R}^{min}, d, D, G_T, M\}$ depends on both reader and implant features and are hence mutually dependent. The other parameter $G_\tau$, relies solely on the implanted antenna.

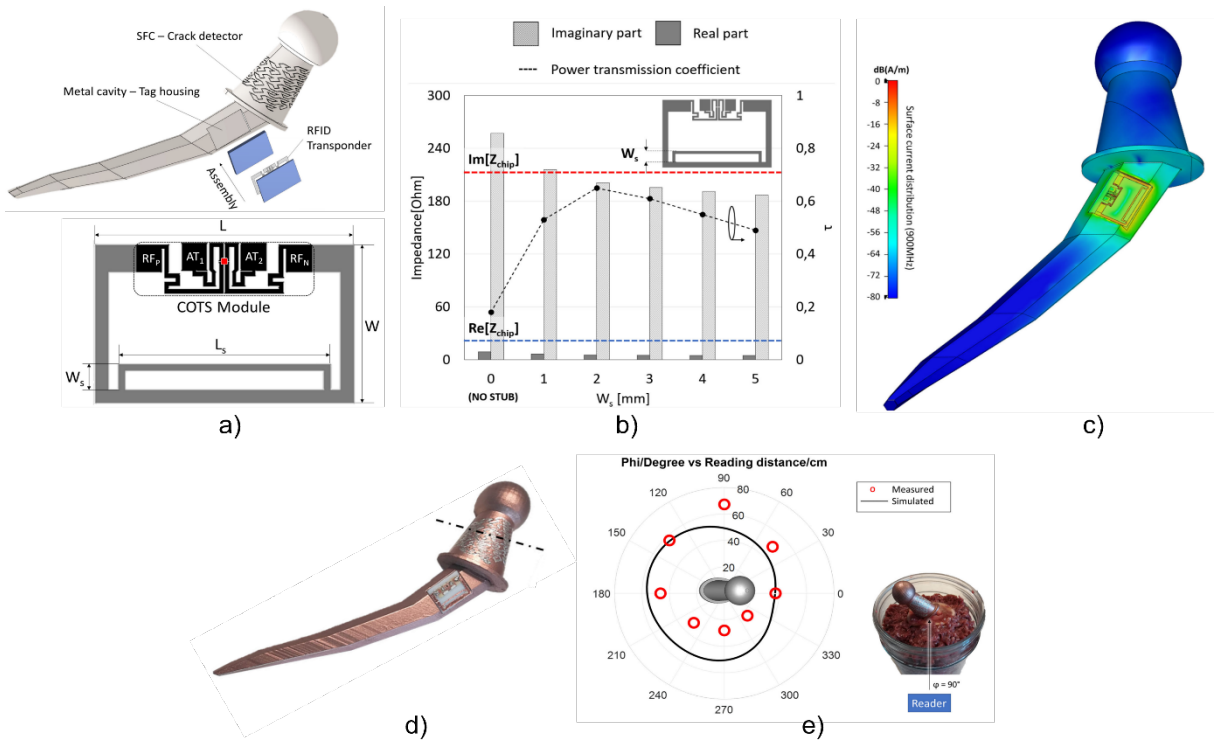


*Figure 3: a) Antennification of a hip-implant through a coupled-loop exciter integrated into a 2mm.-cavity; b) Parametric analysis at 900 MHz of the input impedance of the cavity backed loop w.r.t. the stub length W. Superimposed are the impedance of the IC to be matched and the corresponding power transfer coefficient. c) Simulated Induced current density; d) Final mock-up after the metallization and the integration of cavity backed loop; e) Measured and simulated maximum read distance on the horizontal plane.*

# 3. Metal Implants

## 3.1. Hip Prostheses

Hip prostheses are bulky metal devices generally made of titanium alloy. Electromagnetically, they can be considered extended ground planes acting as the electric walls of cavity-backed antennas. Antennification can involve an adapter, such as a loop (Fig. 3a), integrating the RFID IC into a small notch carved out of the prosthesis [36]. The cavity-backed antenna can be matched to the IC impedance by varying the geometry of the loop, specifically the width $W_S$ of a matching nested stub (Fig. 3b). This primarily controls the imaginary part of the input impedance, while the real part is determined by other parameters chosen based on the stem size [25].
To comply with the metal composition of the hip, the loop can be held apart from the hip notch using a biocompatible dielectric substrate (e.g., PET, polyethylene terephthalate, or PTFE, polytetrafluoroethylene), as shown in Fig. 3a. This configuration requires minimal modification of the standard layout. Currents are primarily concentrated in the loop region (Fig. 3c), while they quickly dissipate in the remaining part of the prosthesis.

The final mock-up of the smart hip prostheses is shown in Fig. 3d. Assuming a radiated power of 3.2 W EIRP, an implantation depth of $d$=5 cm, and $p_C$ =-17.5 dBm numerical and experimental data estimate a read distance of up to $D$=70 cm (Fig. 3e).

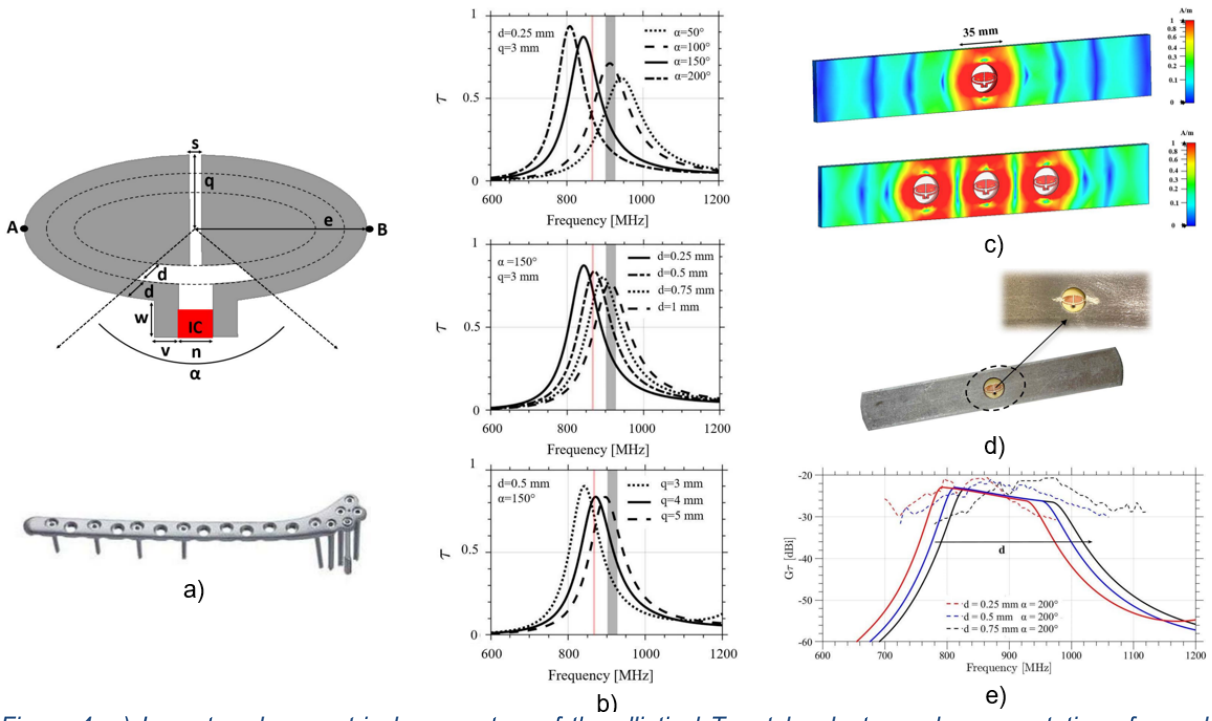


*Figure 4: a) Layout and geometrical parameters of the elliptical T-match adapter and representation of a real bone plate. b) Parametric analysis of the simulated power transfer coefficient versus α, d and q, having case by case kept fixed the other parameters. c) Simulated surface current density at 868 MHz for single and multiple harvesters. d) Prototype of the sensorized fixation plate. e) Measured and simulated realized gain along the normal axis of the plate for different values of the tuning parameter d.*

## 3.2. Bone Plates

Bone plates are titanium or stainless-steel fixators that hold fractured bone fragments together. These devices are conventionally fixed to biological tissues with screws through holes. Depending on the specific bones, some holes may be unused, allowing an antenna adapter to be placed in one of them forming a nested T-match for antennification [37]. In this design, the adpter comprises a PCB disk hosting two concentric metallic ellipses forming a slot-line stub to provide impedance tuning for the hosted RFID IC (Fig. 4a). The tuning parameters investigated include the stub width $d$, the minor semiaxis of the external ellipse $q$, and the aperture angle α, determining the length of the stubs. This layout allows for two-level peak frequency tuning, both coarse and fine (Fig. 4b).

The disk module is electrically connected to the hole boundaries to promote the excitation of the entire implantable device. The simulated surface current density exhibits oscillations that quickly dissipate due to the high losses of the surrounding human tissues (Fig. 4.c). Therefore, the active region for radiation is concentrated near the hole, resembling that of an implanted flat dipole of length 35 mm. If more than one hole is unused, these can be equipped with multiple adapters to achieve a multi-point/ distributed sensing of the bone (Fig. 4.c). A prototype (Fig. 4.d) was tested using a realistic setup comprising a cow bone and a phantom made by a cylinder filled by minced meat. Measurements and simulations agreed on a realized gain of $G_\tau = -25dB$ that would enable a maximum read distance D=40cm when the implant is placed at a depth d=4cm (Fig. 4.e).

## 4. Linear Metal Implants

### 4.1. Vascular Stent

A stent is a metal-mesh tubular device used to treat stenosis, an abnormal narrowing of blood vessels due to the atypical accumulation of atherosclerotic plaque [38]. Made of biocompatible metal alloys, such as Nitinol, which has good conducting properties, the stent is a natural candidate to act as a structural antenna with minimal geometric changes, ensuring its structural stability.

Typical vascular stents have an elongated shape, making them similar to wire antennas. This device can be transformed into an asymmetric dipole [39] by adding a protruding Nitinol straight wire at one extremity, which mounts the RFID IC and additional lumped elements for impedance matching (Fig. 5a). The lumped inductor is used to tune the antenna matching in different operative conditions (Fig. 5b). In this case study, the resulting cyber-stent functions as both an antenna and a sensor. Its response (i.e. $P_{av,R}^{min}$) can be tuned by an inductor connected in series to the IC, with the inductor value selected to optimize sensitivity to restenosis—a proliferation of tissue inside or around the medical device that modifies the antenna's local boundary conditions.

An early attempt [39] demonstrated, through numerical and experimental analysis, the possibility of reading the resulting cyber stent up to D=20 cm from the body with an input power to the reader between 25-28 dBm (Fig.5 c) depending on the level of the stenosis. It is worth noting that the antennified stent in this example is not yet practical for real-world applications due to the size and shape of the add-on element (~2 cm).

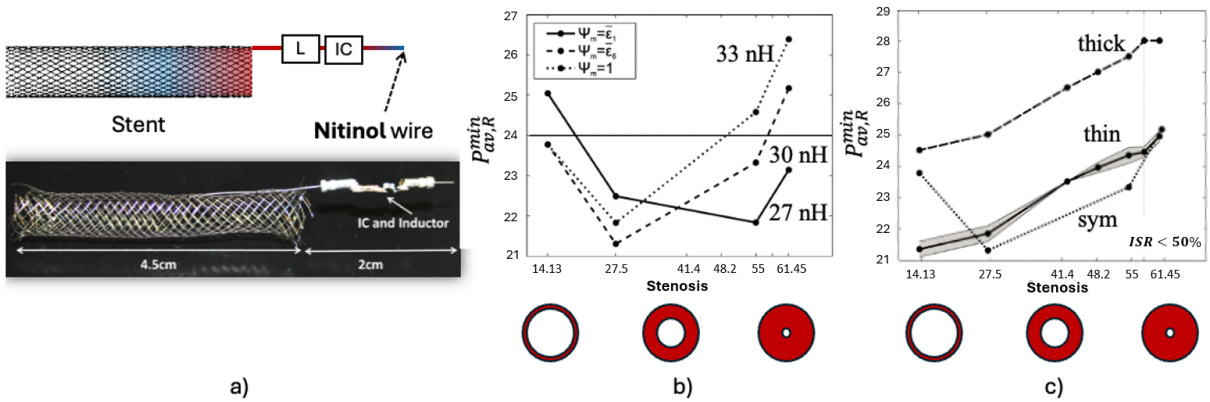


*Figure 5: a) Concept of the STENTag, with current density and prototype. Measured input power at the reader for different level stages of stenosis and b) different tuning inductors and c) different human phantoms.*

### 4.2. Cardiac Valve

Artificial biological valves [40] are replacements for malfunctioning native heart organs. Typically composed of animal-derived semi-lunar-shaped leaflets attached to a supportive structure called a stent, these valves are commonly crafted from metallic alloys that resemble a loop with three cusps acting as meanders (Fig. 6a). Given that the typical size of human cardiac valves is comparable to the wavelength at 900 MHz in the surrounding medium (approximately 5 cm), the stent, when appropriately excited, can support a current pattern resembling that of a typical one-wavelength loop antenna, with in-phase currents in its two half-portions (Fig. 6a).

Antennification without any structural interruption can be achieved by including a trapezoidal loop adapter inductively coupled with one of the cusps, following its geometric profile without any

protrusions (Fig. 6a) [22]. The loop size can be optimized (Fig. 6a) to maximize the Transducer Power Gain by varying the height *h* and the value of the tuning inductor *L*.
Referring to Fig. 6.c, the optimal regions (in white and light grey) are those with $G_T \geq -40$ dB, allowing for multiple configurations.
A prototype using a real heart device was designed and tested in liquid-emulating muscle tissue (Fig. 6d). The trapezoidal exciter was embedded into the same dielectric coating covering the prosthesis, ensuring the structural stability and integrity of both the valve and the lumen. The interrogating antenna was a folded patch (40 mm x 25 mm, as in [41]) placed in contact with the external surface (D=0) of the phantom. Despite the deep implant region (approximately 7 cm from the skin) and the lossy medium surrounding the miniaturized antenna, a robust communication link was achieved with an input power of $P_{av,R}$=1 W for the reader antenna placed in contact with the body. A transducer gain between -37 and -35 dB was measured in the UHF band [30], corresponding to a power margin of 3 dB (Fig. 6e).

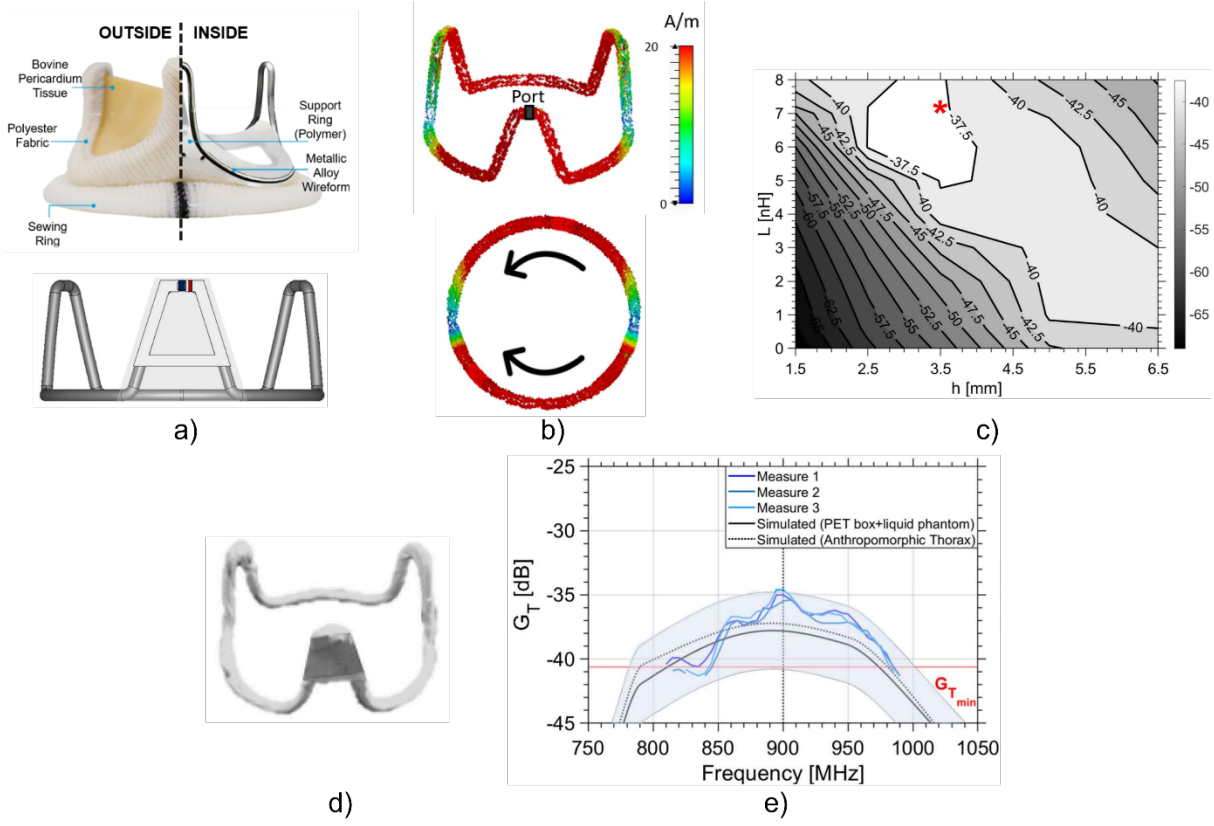


*Figure 6: a) Structure of a biological aortic valve prosthesis with a metallic stent and its cyber equivalent. b) Simulated surface current on the metallic stent of the valve. c) Isolines of the Transducer Power Gain [dB] at 900 MMHz v.s. design parameters of the exciter. The red star represents the selected configuration. d) Prototype and e) simulated and measured $G_T$ vs. frequency*

Some biological valve prostheses can integrate metal-free supporting structures. In such cases, the wire stent is replaced by a polymeric framework to which animal leaflets are connected. The stent structure is then surrounded by a silicone rubber base ring for easy sewing onto the native aortic annulus. With no conductive elements available, the antennification involves integrating a thin antenna into the layout, utilizing the valve materials as a substrate. As an example, the experiment in [15] considered a curvilinear dipole (C-dipole) wrapped around the silicone ring. The dipole is connected to the RFID IC via a triangular T-match that follows the profile of the cusp. The prototype shows an average Transduced Power Gain of –35 dB in the RFID EU band, corresponding to a margin M=6dB, so that the antennified valve can be read by the same contacting antenna (D=0) as above even when implanted at a depth d=7cm.

### 4.3. Orthopedic Nails

Orthopedic nails are used in the treatment of fractures and reconstructive surgery. They are typically composed of bioinert materials, such as stainless steel and titanium, with an elongated shape. The antennification strategy [24] involves replacing one of the extremal screws of the nail with an engineered version that creates a small gap between the metallic portions of the implants. The new end-cap (Fig. 7a) consists of three parts: two metal rods (one screwed inside the nail) and a sandwiched dielectric rod made of biocompatible polymers like polyether ether ketone (PEEK) [42]. A small PCB hosting the IC and a series inductor vertically connects the two metallic rods. This configuration results in an asymmetric dipole with a nearly floating port.

Numerical simulations show that the electric current density induced on the nail flows over the entire device length, fully contributing to the harvesting and radiation phenomena (Fig. 7b). Tests using a 5 cm-long nail within a realistic mock-up (Fig. 7c) showed that the measured realized gain ranges between -30 and -26 dB in the UHF band. This corresponds to a read distance of $D$ = 10 cm for implants placed at a depth of $d$ = 4 cm within the body, considering a low-power reader emitting 1 W (Fig. 7d).

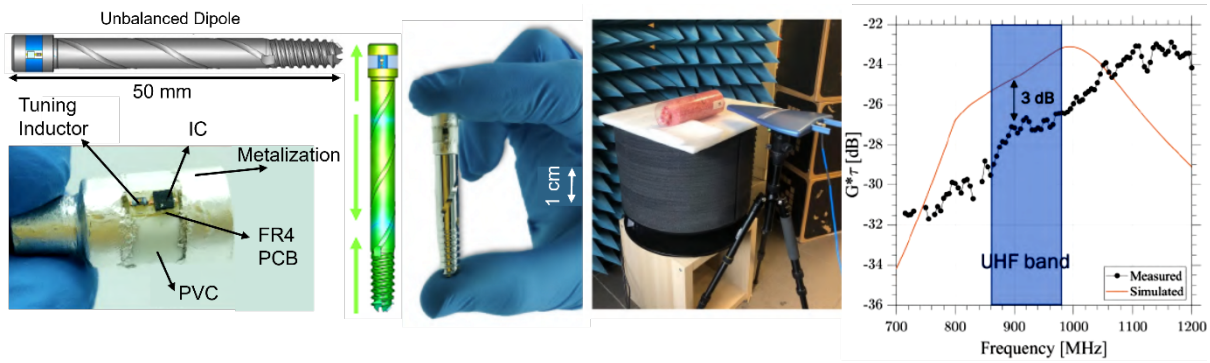


*Figure 7: a) Simulated model of the sensorized End Cap, including the RFID IC, applied on the top of the fixator to achieve an unbalanced dipole. b) Current distribution and prototype c) Measurement setup for the electromagnetic characterization of the prototype inserted into a minced meat phantom. d) Measured and simulated realized gain vs. frequency.*

### 4.4. Tooth implants

A tooth implant is a customized artificial device that replaces a missing tooth to restore masticatory function and aesthetic appearance. To assess the implant success, track its stability and health and evaluate the effectiveness of its action, parameters such as temperature and pressure [43], [44], [45] must be monitored through a telemetry system fully integrated in the small volume of the tooth.

The tooth implant is made of three components: the screw (usually made of titanium for biocompatibility), which replaces of the tooth root, the abutment, made of either metallic or polymeric material, which is placed on top of the dental implant to connect it to the replacement tooth; and finally, the crown, made of ceramic material, which serves as the custom-fabricated replacement tooth.
Following the same concept used for the nail, the screw and the abutment can be engineered [46] to function as an asymmetric harvesting dipole antenna. In this case, the end-cap adapter (Fig. 8a), forming the gap with the medical device, is flattened into a small, thin disk to fit inside the crown. The disk, a PCB with a diameter of 1.2 cm and a thickness of 1.6 mm, hosts two circular segments forming a gap. One of the segments is connected to the abutment. The IC and the tuning inductor are placed in series across the gap, with the inductor value chosen to optimize impedance matching.
Measurements on porcine jaw demonstrated that the antennified tooth can be interrogated from the outside up to D=30 cm with the reader emitting 3.2 W EIRP for continuous overnight monitoring (Fig.8 b-c).

## 5. Materials and Manufacturing

Besides the geometrical and electrical design of the adapter, the antennification of passive prostheses

also requires considering technological issues related to compliance with biocompatibility requirements and, importantly, the manufacturing and integration processes.
For metallic implants, the prosthesis-adapter assembly must be kept together through a biocompatible polymeric coating. This coating aims to avoid dangerous protrusions, movements of the elements, infection, and rejection, and to protect the circuitry from the surrounding human body. Inert materials, such as polyaryletherketones (PEEKs), polyamides (nylons), polysulfones, polyvinylchloride, and polyesters, significantly reduce the probability of infection, a primary cause of implant failure [47].

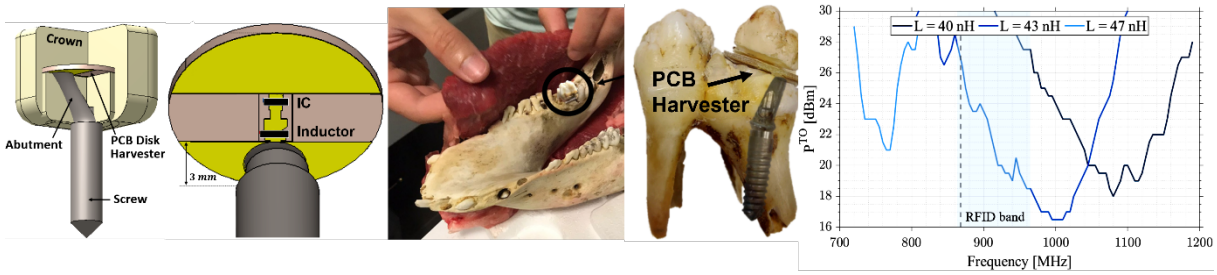


*Figure 8: (a) Cyber-tooth model with the harvester and add-on disk. On the right, the equivalent dipole. (b) Prototype and measurement setup. c) Measured performances for different values of the tuning inductor.*

In the case of polymeric implants, the challenge is incorporating conductive elements that can withstand cyclical strain, bending, and torsion. Various techniques have been developed to embed flexible electronic circuits on dielectric materials, classified into 3D and 2D solutions [48]. The 3D methods use thin wires or conductive threads sewn onto the dielectric, while 2D techniques include ink-jet printing [48], rod coating, and spin-coating of nanomaterials [49]. Conductive polymers suffer from long-term stability issues [50], and graphene/carbon nanotubes face expensive synthesis processes [51]. Conductive paints, such as metallic nanoparticle inks [36], [52], [53], or MXene [54], offer promising electrical performance but lack robustness and contain toxic materials, complicating their medical use. These techniques also require new certifications due to the addition of new materials.
An emerging manufacturing option relies on Laser-induced graphene (LIG) process that patterns conductive traces on high-carbon substrates like polymers. LIG combines graphene's properties—mechanical robustness, electrical conductivity, and biocompatibility — with ease of manufacture and reduced costs [51]. It converts the current substrate into graphene by breaking covalent bonds with an infrared laser [55]. This process requires only a soft requalification of the device. Several LIG sensors on medical-grade polymers have been already reported [49], [56], [57], [58], and their properties are being explored [59], [60] for antenna manufacturing. An implanted square loop antenna on a PEEK substrate shows communication performance with a radiation gain only 3 dB lower than copper in optimal conditions (RS = 5 Ω/□, size 3 cm) [61].
In contrast to the above permanent solutions, a noteworthy research topic involves transient electronics, namely components that gradually dissolve into biofluids after their useful functional life [62]. Despite being in its infancy, this approach could offer a significant advantage over the antennification strategy by providing fully resorbable devices, which could potentially minimize long-term complications. Therefore, materials such as magnesium (Mg) for the conductive traces, magnesium-oxide (MgO) and silicon dioxide ($SiO_2$) working as dielectrics, silk as the substrate, and silicon nanomembranes (semiconductors) have been employed in the past to fabricate RF components, including antennas, lumped components (e.g., resistors, inductors, and capacitors), transistors and even energy harvesting subsystems.

## 6. Conclusion

The presented examples demonstrate that passive implanted prostheses can be effectively transformed into wireless cyber devices for supporting and monitoring the human body, despite the variability in shape and materials. Several recurring design patterns can be identified, allowing for a few antennification strategies to be customized on a case-by-case basis.
Battery-less communications based on backscattering protocols should be preferred to minimize the impact on the human body and optimize biocompatibility. Metallic and polymeric portions of the

implants can be utilized to act as radiating elements or dielectric substrates for radiating elements, respectively. Among the antenna parameters to be optimized for establishing a through-the-body communication link, impedance matching is the most critical one, as the radiation gain is hardly controllable as it is primarily influenced by the prosthesis's shape, size, and implantation depth. Antenna adapters can be efficiently used to integrate the necessary electronics, tune them to the prosthesis impedance, and shape the induced/radiating currents. The coupled-loop family appears to be the most suitable topology, as it requires no interruption or modification of the implant.
The electromagnetic performances achieved so far are resumed in Table II. Deepest implants like heart valves, or very small prosthesis, can be efficiently read from outside, even if in some cases on-skin interrogating antennas are required (in this case exceptional advantages are expected by the usage of wearable readers antenna such as the one in [63], the wristband reader in [64] and the array in [65]). Orthopedic devices, generally larger and implanted more superficially, can be instead interrogated by reader placed far from the skin, hence enabling remote monitoring policies. Furthermore, multi-point or multi-parametric analysis can be performed by including more than a single adapter and hence ICs and sensors.
Finally, the required communication powers are compliant with SAR regulations, being the interrogation duty-cycle low or the distance from the body large.
It is worth noticing that the same approach can be successfully applied to wearable prosthesis [66], but in this case with less effort in energy harvesting, miniaturization, and body acceptance.

*Table 2 Communication features of the described examples*

| Papers | Implantation Depth *d* [mm] | Reader Distance from the Skin [mm] | Chip Sensitivity [dBm] | Power radiated by the reader [W] (Far-field) | Realized Gain [dB] (Far-field) | Transducer Power Gain [dB] (Near-Field) | Power Margin *M* [dB] (Near-Field) | SAR max [W/kg] |
|---|---|---|---|---|---|---|---|---|
| [36] | 70 | 70 | -17.5 | 3.2 EIRP | -27 | - | - | 0.25 (duty cycle=1) |
| [46] | 10 | 2 | -16.6 | 3.2 EIRP | -24 | - | - | - |
| [39] | 17 | 200 | -15 | 1 EIRP | - | - | - | - |
| [22] | 70 | 2 | -13.6 | - | - | -37 | 3.5 | 2 (duty cycle=0.11) |
| [24] | 40 | 100 | -13.6 | 1 EIRP | -24 | - | - | - |
| [37] | 40 | 300 | -13.6 | 3.2 W EIRP | -22 | - | - | - |
| [15] | 70 | 2 | -13.6 | - | - | -35 | 6 | 2 (duty cycle=0.11) |

However, several critical points remain still open and require further investigation. In-vivo testing is essential to validate the long-term performance and biocompatibility of these cyber-prostheses under realistic physiological and pathological conditions. Particular attention should be devoted to Magnetic Resonance Imaging (MRI) compatibility. Since the layout, materials, and placements [67] of the prosthesis remain largely unaffected during the “antennification” process, the considerations regarding MRI compliance for standard implants are still applicable to their “cyber” versions. However, additional analysis is necessary to ensure the RFID IC and electronic components are compatible with the high magnetic fields generated during MRI. The problem has been already addressed in [68] and RFID tags, containing conductive materials, must be MR-conditional, meaning they are safe under specific conditions during MRI scans. Potential risks include not negligible temperature increases (up to 3°C) and unexpected strong movements. Image artifacts might also occur [69] as well. Recently, MRI-compliant ICs and tags have been developed [70] for textile and wearable applications, and we can expect potential benefits for implantable systems too.

Additionally, the durability of the integrated antennas and electronic components must be ensured to withstand the mechanical stresses and environmental conditions within the human body.
Another significant concern is cybersecurity. As these devices become more interconnected, safeguarding the integrity and privacy of the transmitted data is paramount. Implementing stringent authentication mechanisms at physical level will be crucial to protect against unauthorized access and data breaches.

## Acknowledgements

Work partly funded by European Union - NextGenerationEU, ECS 0000024 Rome Technopole, CUP B83C22002820006, PNRR Mission 4, Component 2, Investment 1.5.

## References

[1] R. Bashirullah, "Wireless Implants," *IEEE Microw Mag*, vol. 11, no. 7, pp. S14–S23, Dec. 2010, doi: 10.1109/MMM.2010.938579.

[2] M. Veletić *et al.*, "Implants with Sensing Capabilities," *Chem Rev*, vol. 122, no. 21, pp. 16329–16363, Nov. 2022, doi: 10.1021/acs.chemrev.2c00005.

[3] J. Andreu-Perez, D. R. Leff, H. M. D. Ip, and G.-Z. Yang, "From Wearable Sensors to Smart Implants—Toward Pervasive and Personalized Healthcare," *IEEE Trans Biomed Eng*, vol. 62, no. 12, pp. 2750–2762, Dec. 2015, doi: 10.1109/TBME.2015.2422751.

[4] K. Misch and H.-L. Wang, "Implant Surgery Complications: Etiology and Treatment," *Implant Dent*, vol. 17, no. 2, pp. 159–168, Jun. 2008, doi: 10.1097/ID.0b013e3181752f61.

[5] N. Li, Z. Jiang, R. Pu, D. Zhu, and G. Yang, "Implant failure and associated risk factors of transcrestal sinus floor elevation: A retrospective study," *Clin Oral Implants Res*, vol. 34, no. 1, pp. 66–77, Jan. 2023, doi: 10.1111/clr.14020.

[6] A. Bilir and S. Dumanli, "In-body Antenna Design for Next Generation Hip Implants," in *2023 24th International Conference on Applied Electromagnetics and Communications (ICECOM)*, IEEE, Sep. 2023, pp. 1–4. doi: 10.1109/ICECOM58258.2023.10367966.

[7] J. Wang, J. Chu, J. Song, and Z. Li, "The application of impantable sensors in the musculoskeletal system: a review," *Front Bioeng Biotechnol*, vol. 12, Jan. 2024, doi: 10.3389/fbioe.2024.1270237.

[8] J. H. Lim *et al.*, "Synthesis of shape-programmable elastomer for a bioresorbable, wireless nerve stimulator," *Biosens Bioelectron*, vol. 254, p. 116222, Jun. 2024, doi: 10.1016/j.bios.2024.116222.

[9] J. Minguillon *et al.*, "Powering Electronic Implants by High Frequency Volume Conduction: In Human Validation," *IEEE Trans Biomed Eng*, vol. 70, no. 2, pp. 659–670, Feb. 2023, doi: 10.1109/TBME.2022.3200409.

[10] C. Xiao, S. Hao, D. Cheng, and C. Liao, "Safety Enhancement by Optimizing Frequency of Implantable Cardiac Pacemaker Wireless Charging System," *IEEE Trans Biomed Circuits Syst*, vol. 16, no. 3, pp. 372–383, Jun. 2022, doi: 10.1109/TBCAS.2022.3170575.

[11] G. Marrocco and L. Mattioni, "Naval Structural Antenna Systems for Broadband HF Communications," *IEEE Trans Antennas Propag*, vol. 54, no. 4, pp. 1065–1073, Apr. 2006, doi: 10.1109/TAP.2006.872559.

[12] V. Makarovaite, A. J. R. Hillier, S. J. Holder, C. W. Gourlay, and J. C. Batchelor, "Passive UHF RFID Voice Prosthesis Mounted Sensor for Microbial Growth Detection," *IEEE Journal of Radio Frequency Identification*, vol. 4, no. 4, pp. 384–390, Dec. 2020, doi: 10.1109/JRFID.2020.3011900.

[13] A. Vena, S. Cahuzac, S. Dutrieux, B. Sorli, and S. Naudi, "Implant-Based UHF RFID-Enabled Sensor to Detect Loosening of Knee Prosthesis," *IEEE Journal of Radio Frequency Identification*, vol. 7, pp. 536–546, 2023, doi: 10.1109/JRFID.2023.3296791.

[14] V. Mazzaracchio, L. Fiore, S. Nappi, G. Marrocco, and F. Arduini, "Medium-distance affordable, flexible and wireless epidermal sensor for pH monitoring in sweat," *Talanta*, vol. 222, p. 121502, Jan. 2021, doi: 10.1016/j.talanta.2020.121502.

[15] F. Naccarata and G. Marrocco, "Integrated Wireless RFID Temperature Sensor for Biological Aortic Valve Prostheses," *IEEE Journal of Radio Frequency Identification*, vol. 7, pp. 293–300, 2023, doi: 10.1109/JRFID.2023.3264557.

[16] A. B. Barba *et al.*, "Miniaturized and Battery-Free Temperature and Humidity Sensor for Smart Pharmaceutical Packaging," *IEEE Journal of Radio Frequency Identification*, vol. 7, pp. 547–555, 2023, doi: 10.1109/JRFID.2023.3312811.

[17] Asygn, "AS3213S - Strain sensor," https://asygn.com/as3213s-strain/.

[18] L. Fiore *et al.*, "Microfluidic paper-based wearable electrochemical biosensor for reliable cortisol detection in sweat," *Sens Actuators B Chem*, vol. 379, p. 133258, Mar. 2023, doi: 10.1016/j.snb.2022.133258.

[19] F. Nanni and G. Marrocco, "Constrained Design of Potentiometric RFID Sensors Based on Auto-Tuning ICs," *IEEE Sens J*, vol. 23, no. 3, pp. 3050–3058, Feb. 2023, doi: 10.1109/JSEN.2022.3226522.

[20] J. Li, Y. Dong, J. H. Park, and J. Yoo, "Body-coupled power transmission and energy harvesting," *Nat Electron*, vol. 4, no. 7, pp. 530–538, Jun. 2021, doi: 10.1038/s41928-021-00592-y.

[21] K. Kwon *et al.*, "A battery-less wireless implant for the continuous monitoring of vascular pressure, flow rate and temperature," *Nat Biomed Eng*, vol. 7, no. 10, pp. 1215–1228, Apr. 2023, doi: 10.1038/s41551-023-01022-4

[22] F. Naccarata, C. Occhiuzzi, R. Verzicco, and G. Marrocco, "Wireless and Zero-Power Trans-Cardiac Link With Antennified Aortic Valve Bioprostheses," *IEEE J Electromagn RF Microw Med Biol*, vol. 7, no. 1, pp. 15–23, Mar. 2023, doi: 10.1109/JERM.2022.3223035.

[23] F. Naccarata, M. Di Cristofano, and G. Marrocco, "Continuous Detection of Fluid Leaks Into the Body by Means of Partially Dissolvable Antennas," *IEEE J Electromagn RF Microw Med Biol*, vol. 8, no. 1, pp. 15–25, Mar. 2024, doi: 10.1109/JERM.2024.3363509.

[24] C. Miozzi, S. Amendola, C. Occhiuzzi, and G. Marrocco, “Augmented Implanted Orthopedic Fixators with an Embedded Temperature Sensor for Early Detection of Deep Infections,” in *2023 IEEE SENSORS*, IEEE, Oct. 2023, pp. 01–04. doi: 10.1109/SENSORS56945.2023.10325069.
[25] G. Marrocco, “The art of UHF RFID antenna design: impedance-matching and size-reduction techniques,” *IEEE Antennas Propag Mag*, vol. 50, no. 1, pp. 66–79, Feb. 2008, doi: 10.1109/MAP.2008.4494504.
[26] R. Lodato and G. Marrocco, “Close Integration of a UHF-RFID Transponder Into a Limb Prosthesis for Tracking and Sensing,” *IEEE Sens J*, vol. 16, no. 6, pp. 1806–1813, Mar. 2016, doi: 10.1109/JSEN.2015.2503887.
[27] T. Wu, T. S. Rappaport, and C. M. Collins, “The human body and millimeter-wave wireless communication systems: Interactions and implications,” in *2015 IEEE International Conference on Communications (ICC)*, IEEE, Jun. 2015, pp. 2423–2429. doi: 10.1109/ICC.2015.7248688.
[28] S. J. Orfanidis, “Electromagnetic waves and antennas,” 2002.
[29] R. Lodato, V. Lopresto, R. Pinto, and G. Marrocco, “Numerical and Experimental Characterization of Through-the-Body UHF-RFID Links for Passive Tags Implanted Into Human Limbs,” *IEEE Trans Antennas Propag*, vol. 62, no. 10, pp. 5298–5306, Oct. 2014, doi: 10.1109/TAP.2014.2345586.
[30] Global Standards Committee (GS1), “Overview of UHF frequency allocations (860 to 930 MHz) for RAIN RFID,” https://www.gs1.org/docs/epc/uhf_regulations.pdf.
[31] I. C. on N.-I. R. Protection, “GUIDELINES FOR LIMITING EXPOSURE TO TIME-VARYING ELECTRIC, MAGNETIC, AND ELECTROMAGNETIC FIELDS (UP TO 300 GHz),” *Health Phys*, vol. 74, no. 4, 1998, [Online]. Available: https://journals.lww.com/health-physics/fulltext/1998/04000/guidelines_for_limiting_exposure_to_time_varying.13.aspx
[32] P. V. Nikitin, K. V. S. Rao, R. Martinez, and S. F. Lam, “Sensitivity and Impedance Measurements of UHF RFID Chips,” *IEEE Trans Microw Theory Tech*, vol. 57, no. 5, pp. 1297–1302, May 2009, doi: 10.1109/TMTT.2009.2017297.
[33] M. C. Caccami and G. Marrocco, “Electromagnetic Modeling of Self-Tuning RFID Sensor Antennas in Linear and Nonlinear Regimes,” *IEEE Trans Antennas Propag*, vol. 66, no. 6, pp. 2779–2787, Jun. 2018, doi: 10.1109/TAP.2018.2820322.
[34] C. A. Balanis, *Antenna theory: analysis and design*. John wiley & sons, 2016.
[35] C. Occhiuzzi, M. Simiele, R. Lodato, and G. Marrocco, “Feasibility, limitations and potentiality of UHF-RFID passive implants,” in *2012 IEEE International Conference on RFID-Technologies and Applications (RFID-TA)*, IEEE, Nov. 2012, pp. 40–45. doi: 10.1109/RFID-TA.2012.6404557.
[36] S. Nappi, L. Gargale, F. Naccarata, P. P. Valentini, and G. Marrocco, “A Fractal-RFID Based Sensing Tattoo for the Early Detection of Cracks in Implanted Metal Prostheses,” *IEEE J Electromagn RF Microw Med Biol*, vol. 6, no. 1, pp. 29–40, Mar. 2022, doi: 10.1109/JERM.2021.3108945.
[37] P. Avaltroni, S. Nappi, and G. Marrocco, “Antennifying Orthopedic Bone-Plate Fixtures for the Wireless Monitoring of Local Deep Infections,” *IEEE Sens J*, vol. 21, no. 18, pp. 21012–21021, Sep. 2021, doi: 10.1109/JSEN.2021.3097448.
[38] L. Shedden, S. Kennedy, R. Wadsworth, and P. Connolly, “Towards a self-reporting coronary artery stent—Measuring neointimal growth associated with in-stent restenosis using electrical impedance techniques,” *Biosens Bioelectron*, vol. 26, no. 2, pp. 661–666, Oct. 2010, doi: 10.1016/j.bios.2010.06.073.
[39] C. Occhiuzzi and G. Marrocco, “Experimental characterization of the RFID STENTag for passive vascular monitoring,” in *2012 6th European Conference on Antennas and Propagation (EUCAP)*, IEEE, Mar. 2012, pp. 3669–3671. doi: 10.1109/EuCAP.2012.6206153.
[40] P. Blanke *et al.*, “Computed tomography assessment for transcatheter aortic valve in valve implantation: The vancouver approach to predict anatomical risk for coronary obstruction and other considerations,” *J Cardiovasc Comput Tomogr*, vol. 10, no. 6, pp. 491–499, Nov. 2016, doi: 10.1016/j.jcct.2016.09.004.
[41] C. Miozzi, G. Saggio, E. Gruppioni, and G. Marrocco, “Constrained Safety-Integrity Performance of Through-the-Arms UHF-RFID Transcutaneous Wireless Communication for the Control of Prostheses,” *IEEE Journal of Radio Frequency Identification*, vol. 3, no. 4, pp. 236–244, Dec. 2019, doi: 10.1109/JRFID.2019.2921097.
[42] H. Ma *et al.*, “PEEK (Polyether-ether-ketone) and its composite materials in orthopedic implantation,” *Arabian Journal of Chemistry*, vol. 14, no. 3, p. 102977, Mar. 2021, doi: 10.1016/j.arabjc.2020.102977.
[43] J. J. Kim, G. R. Stafford, C. Beauchamp, and S. A. Kim, “Development of a Dental Implantable Temperature Sensor for Real-Time Diagnosis of Infectious Disease,” *Sensors*, vol. 20, no. 14, p. 3953, Jul. 2020, doi: 10.3390/s20143953.
[44] X. Kang, Y. Li, Y. Wang, Y. Zhang, D. Yu, and Y. Peng, “Relationships of Stresses on Alveolar Bone and Abutment of Dental Implant from Various Bite Forces by Three-Dimensional Finite Element Analysis,” *Biomed Res Int*, vol. 2020, pp. 1–9, Feb. 2020, doi: 10.1155/2020/7539628.
[45] S. Vellappally, A. A. Al Kheraif, D. D. Divakar, S. Basavarajappa, S. Anil, and H. Fouad, “Tooth implant prosthesis using ultra low power and low cost crystalline carbon bio-tooth sensor with hybridized data acquisition algorithm,” *Comput Commun*, vol. 148, pp. 176–184, Dec. 2019, doi: 10.1016/j.comcom.2019.09.020.
[46] N. Panunzio *et al.*, “Cyber-Tooth: Antennified Dental Implant for RFID Wireless Temperature Monitoring,” in *2021 IEEE International Conference on RFID Technology and Applications (RFID-TA)*, IEEE, Oct. 2021, pp. 211–214. doi: 10.1109/RFID-TA53372.2021.9617316.
[47] A. Pandey and S. Sahoo, “Progress on Medical Implant: A Review and Prospects,” *J Bionic Eng*, vol. 20, no. 2, pp. 470–494, Mar. 2023, doi: 10.1007/s42235-022-00284-z.

[48] S. Naghdi, K. Y. Rhee, D. Hui, and S. J. Park, "A Review of Conductive Metal Nanomaterials as Conductive, Transparent, and Flexible Coatings, Thin Films, and Conductive Fillers: Different Deposition Methods and Applications," *Coatings*, vol. 8, no. 8, p. 278, Aug. 2018, doi: 10.3390/coatings8080278.
[49] S. P. Singh, Y. Li, J. Zhang, J. M. Tour, and C. J. Arnusch, "Sulfur-Doped Laser-Induced Porous Graphene Derived from Polysulfone-Class Polymers and Membranes," *ACS Nano*, vol. 12, no. 1, pp. 289–297, Jan. 2018, doi: 10.1021/acsnano.7b06263.
[50] H. Yoon and J. Jang, "Conducting-Polymer Nanomaterials for High-Performance Sensor Applications: Issues and Challenges," *Adv Funct Mater*, vol. 19, no. 10, pp. 1567–1576, May 2009, doi: 10.1002/adfm.200801141.
[51] C. Soldano, A. Mahmood, and E. Dujardin, "Production, properties and potential of graphene," *Carbon N Y*, vol. 48, no. 8, pp. 2127–2150, Jul. 2010, doi: 10.1016/j.carbon.2010.01.058.
[52] C. Liu *et al.*, "3D Printing Technologies for Flexible Tactile Sensors toward Wearable Electronics and Electronic Skin," *Polymers (Basel)*, vol. 10, no. 6, p. 629, Jun. 2018, doi: 10.3390/polym10060629.
[53] S. Guo, K. Qiu, F. Meng, S. H. Park, and M. C. McAlpine, "3D Printed Stretchable Tactile Sensors," *Advanced Materials*, vol. 29, no. 27, Jul. 2017, doi: 10.1002/adma.201701218.
[54] J. A. Kumar *et al.*, "Methods of synthesis, characteristics, and environmental applications of MXene: A comprehensive review," *Chemosphere*, vol. 286, p. 131607, Jan. 2022, doi: 10.1016/j.chemosphere.2021.131607.
[55] R. Ye, D. K. James, and J. M. Tour, "Laser-Induced Graphene: From Discovery to Translation," *Advanced Materials*, vol. 31, no. 1, Jan. 2019, doi: 10.1002/adma.201803621.
[56] A. Lamberti *et al.*, "All-SPEEK flexible supercapacitor exploiting laser-induced graphenization," *2d Mater*, vol. 4, no. 3, p. 035012, Jul. 2017, doi: 10.1088/2053-1583/aa790e.
[57] J. Wang, N. Wang, D. Xu, L. Tang, and B. Sheng, "Flexible humidity sensors composed with electrodes of laser induced graphene and sputtered sensitive films derived from poly(ether-ether-ketone)," *Sens Actuators B Chem*, vol. 375, p. 132846, Jan. 2023, doi: 10.1016/j.snb.2022.132846.
[58] A. K. Thakur, H. Mahbub, F. H. Nowrin, and M. Malmali, "Highly Robust Laser-Induced Graphene (LIG) Ultrafiltration Membrane with a Stable Microporous Structure," *ACS Appl Mater Interfaces*, vol. 14, no. 41, pp. 46884–46895, Oct. 2022, doi: 10.1021/acsami.2c09563.
[59] A. Mostaccio, G. Antonelli, M. Bragaglia, E. Martinelli, and G. Marrocco, "Comparative Evaluation of Laser-Induced Graphene (LIG) Traces on Polyimide Under Soft and Hard Stress for IoT Applications," *IEEE Journal on Flexible Electronics*, vol. 2, no. 3, pp. 256–264, 2023.
[60] A. Mostaccio, F. Naccarata, F. M. C. Nanni, J. Filippi, E. Martinelli, and G. Marrocco, "Soft and Flexible Wireless Epidermal Plaster Made by Laser-Induced Graphene," *IEEE Sens Lett*, 2024.
[61] F. Naccarata, A. Mostaccio, J. Filippi, E. Martinelli, and G. Marrocco, "Upper-Bound Performance of Laser-Induced Graphene (LIG) Antennas on PEEK for Implantable Applications," in *2024 IEEE International Symposium on Antennas and Propagation (AP-S)*, Florence, Jul. 2024.
[62] S. Hwang *et al.*, "Materials for Bioresorbable Radio Frequency Electronics," *Advanced Materials*, vol. 25, no. 26, pp. 3526–3531, Jul. 2013, doi: 10.1002/adma.201300920.
[63] S. Ahmed, D. Le, L. Sydanheimo, L. Ukkonen, and T. Bjorninen, "Wearable Metasurface-Enabled Quasi-Yagi Antenna for UHF RFID Reader With End-Fire Radiation Along the Forearm," *IEEE Access*, vol. 9, pp. 77229–77238, 2021, doi: 10.1109/ACCESS.2021.3078239.
[64] G. M. Bianco, S. Amendola, and G. Marrocco, "Near-Field Constrained Design for Self-Tuning UHF-RFID Antennas," *IEEE Trans Antennas Propag*, vol. 68, no. 10, pp. 6906–6911, Oct. 2020, doi: 10.1109/TAP.2020.2995315.
[65] C. Miozzi, G. Saggio, E. Gruppioni, and G. Marrocco, "Near-Field Circular Array for the Transcutaneous Telemetry of UHF RFID-Based Implantable Medical Devices," *IEEE J Electromagn RF Microw Med Biol*, vol. 6, no. 2, pp. 219–227, Jun. 2022, doi: 10.1109/JERM.2021.3111128.
[66] M. Wagih *et al.*, "Microwave-Enabled Wearables: Underpinning Technologies, Integration Platforms, and Next-Generation Roadmap," *IEEE Journal of Microwaves*, vol. 3, no. 1, pp. 193–226, Jan. 2023, doi: 10.1109/JMW.2022.3223254.
[67] I. A. Shah, Y. Cho, and H. Yoo, "Safety Evaluation of Medical Implants in the Human Body for a Wireless Power Transfer System in an Electric Vehicle," *IEEE Trans Electromagn Compat*, vol. 63, no. 3, pp. 681–691, Jun. 2021, doi: 10.1109/TEMC.2020.3023734.
[68] Fujitsu, "Recommended MRI labeling based on the test results," https://www.fujitsu.com/us/Images/Fujitsu_WT-A533_RFID_Recommended_MRI_Labeling_Updated_%2010-5-17_%28for%20Customers%29.pdf.
[69] K. D. Kurz, Ø. Kallevåg, K. Austrått, B. Styr, J. B. Leiknes, and P. Krøger, "Artifacts on Magnetic Resonance Imaging from Electronic Identification Enablement in Silicone Gel Implants Are Not Negligible," *Plast Reconstr Surg Glob Open*, vol. 9, no. 11, p. e3941, Nov. 2021, doi: 10.1097/GOX.0000000000003941.
[70] Datamars, "Datamars releases a whitepaper on the use of RFID transponders in MRI scanners," https://datamars.com/2020/08/01/datamars-releases-a-whitepaper-on-the-use-of-rfid-transponders-in-mri-scanners/.